

Superconducting transport through a vibrating molecule

A. Zazunov,^{1,2} R. Egger,^{1,3} C. Mora,^{1,3} and T. Martin^{1,4}

¹ *Centre de Physique Théorique, Case 907 Luminy, F-13288 Marseille cedex 9, France*

² *LPMMC CNRS, 25 av. des Martyrs, F-38042 Grenoble, France*

³ *Institut für Theoretische Physik, Heinrich-Heine-Universität, D-40225 Düsseldorf, Germany*

⁴ *Université de la Méditerranée, F-13288 Marseille cedex 9, France*

(Dated: June 24, 2018)

Nonequilibrium electronic transport through a molecular level weakly coupled to a single coherent phonon/vibration mode has been studied for superconducting leads. The Keldysh Green function formalism is used to compute the current for the entire bias voltage range. In the subgap regime, Multiple Andreev Reflection (MAR) processes accompanied by phonon emission cause rich structure near the onset of MAR channels, including an even-odd parity effect that can be interpreted in terms of an inelastic MAR ladder picture. Thereby we establish a connection between the Keldysh formalism and the Landauer scattering approach for inelastic MAR.

PACS numbers: 74.78.Na, 74.45.+c, 74.50.+r

I. INTRODUCTION

One of the primary goals in the field of molecular electronics is to understand quantum transport through individual nanoscale objects, such as molecules, short carbon nanotubes, or DNA; for reviews, see Refs. [1, 2, 3]. An important difference to conventional mesoscopic transport through quantum dots or granular islands arises because molecules can have intrinsic vibrational degrees of freedom ('phonons') that may give rise to Franck-Condon sidebands or phonon blockade in electronic transport. Such features have been studied theoretically in many recent papers [4, 5, 6, 7, 8]. Molecular electronics is particularly exciting because it is in principle possible to contact molecules by leads of different nature. Here we discuss how nonequilibrium transport is affected by a coherent phonon mode coupled to the molecular charge for the case of (*s*-wave BCS) *superconducting leads*. Molecules connected to superconductors promise a rich terrain of exploration that allows for new spectroscopic tools (probing molecular properties), potentially useful applications, and interesting fundamental physics. First experimental results have appeared for carbon nanotubes [9, 10, 11, 12, 13] and metallofullerenes [14].

So far transport through molecules has been theoretically studied only for normal leads, either using rate equations or (in the quantum-coherent regime) perturbation theory in the electron-phonon coupling λ [7]. For superconducting leads and large transmission through the molecule, subgap transport is ruled by MAR processes [15, 16]. These have been extensively studied for point contacts [17, 18, 19] and for junctions containing a resonant level [20, 21]. In this paper, we provide a theoretical framework to include vibrations into superconducting transport through a resonant molecular level. We focus on the most interesting quantum-coherent low temperature (T) limit with high (bare) transmission, where Coulomb charging effects are largely wiped out. Therefore the Coulomb interaction on the molecule will be neglected here. We compute the d.c. current basically for

the full bias (V) range within a Keldysh Green function scheme valid for small λ but arbitrary phonon frequency ω_0 . This approximation is current-conserving for identical molecule-lead couplings $\Gamma_L = \Gamma_R = \Gamma$ and superconductor gaps $\Delta_L = \Delta_R = \Delta$.

Our main results are as follows. (i) For $eV \gg \Delta$, the coupling λ tends to *enhance* the excess current I_{exc} , which is defined as the difference in current for $V \rightarrow \infty$ when changing normal into superconducting leads. (ii) In the subgap regime $eV < 2\Delta$, the phonon gives rise to a quite complicated structure in the I - V characteristics around each MAR onset at $eV = 2\Delta/n$ (integer n), with a pronounced *even-odd parity* dependence. These results can be qualitatively understood within a MAR ladder picture. Such a picture has previously been used for junctions with a resonant level [21] and is here extended to include phonon-induced transitions (inelastic MAR). Rich features in the I - V curve appear already for $eV \ll \hbar\omega_0$, in contrast to normal leads where phonon signatures (e.g. sidebands) emerge only at $eV \geq \hbar\omega_0$ [5, 7]. (iii) For $V = 0$, we give analytical results for the Josephson current in the adiabatic limit, $\hbar\omega_0 \ll \Delta \ll \Gamma$. We find a reduction (but no destruction) of the critical current and a changed current-phase relation. These findings are in qualitative agreement with Ref. [22], where the opposite limit $\Gamma \ll \Delta$ has been studied by lowest-order perturbation theory in the lead-molecule hopping.

The outline of the paper is as follows. In Sec. II, we discuss the model and the Keldysh Green function approach taken in this work. In Sec. III, we present our results and provide a physical interpretation in terms of a MAR ladder picture. How such a scattering-type approach can be connected to the Keldysh approach is explained in detail in the Appendix. Finally, some conclusions are offered in Sec. IV. We put $e = \hbar = 1$ in intermediate steps.

II. MODEL AND KELDYSH APPROACH

A. Model

We now wish to formulate and analyze a tractable model describing the relevant physics of a molecule sandwiched between superconducting leads. Writing the Hamiltonian as

$$H = \omega_0 b^\dagger b + \sum_{\sigma} (\epsilon_0 + \lambda X) d_{\sigma}^{\dagger} d_{\sigma} + H_L + H_R + H_T, \quad (1)$$

we consider one relevant molecular level associated with the fermion operator d_{σ} for spin $\sigma = \uparrow, \downarrow$ and located at the energy ϵ_0 . In Eq. (1) we take a linear coupling between the molecular charge and the phonon displacement $X = b + b^\dagger$, where the boson operator b annihilates a phonon excitation. For a justification of this form and possible other couplings, see Ref. [5]. The leads are described by a pair of standard s -wave BCS Hamiltonians. Using the Nambu vector $\Psi_{j,k}^T = (\psi_{j,k,\uparrow}, \psi_{j,-k,\downarrow}^{\dagger})$ for electrons in lead $j = L/R$, we have

$$H_{j=L/R} = \sum_k \Psi_{jk}^{\dagger} \begin{pmatrix} \xi_k & \Delta \\ \Delta^* & -\xi_k \end{pmatrix} \Psi_{jk} \quad (2)$$

with single-particle energy $\xi_k = k^2/2m - \epsilon_F$; the 2×2 matrix acts in Nambu space. In the following, standard Pauli matrices in Nambu space are used and denoted by $\sigma_{x,y,z}$. Using the Nambu vector $d = (d_{\uparrow}, d_{\downarrow}^{\dagger})^T$ and $\Gamma = \pi\nu_0|t_0|^2$ for (normal) lead density of states ν_0 , the lead-molecule coupling is

$$H_T = t_0 \sum_{k,j=L/R=\pm} \Psi_{jk}^{\dagger} \sigma_z e^{\pm i\sigma_z V t/2} d + \text{h.c.}, \quad (3)$$

where the voltage V enters via the time-dependent phase. As we are mostly interested in the $V \neq 0$ case, for simplicity, we consider $\Delta > 0$ to be real-valued. (In the study of the Josephson current, the residual $V = 0$ phase difference across the molecule is of course taken into account.)

Note that Eqs. (2) and (3) assume symmetric coupling and identical superconducting gaps. Our approximation scheme below will yield a current-conserving result only then. In fact, since the calculation of MAR-dominated transport is already involved for $\lambda = 0$, a nontrivial current-conserving self-consistent approach covering the large transmission limit seems out of question. Note that self-consistency is (usually) sufficient to ensure current conservation [23]. Below we instead proceed using a perturbation theory with the small expansion parameter λ/Γ . Under such an approach, current conservation is known to only hold for the electron-hole symmetric case [24], i.e., $\epsilon_0 = 0$, with symmetrically arranged leads ($\Delta_L = \Delta_R = \Delta, \Gamma_L = \Gamma_R = \Gamma$). This case is taken in what follows. We note in passing that this important issue (and also the tadpole diagram in Fig. 1) was

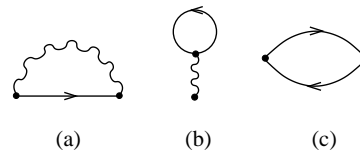


FIG. 1: Self energy due to the presence of the phonon mode: (a) 'Fock' and (b) 'tadpole' diagram. The polarization bubble (c) leads to the dressed phonon propagator $\tilde{\mathcal{D}}$ (wiggly lines). Arrowed lines denote $\tilde{\mathcal{G}}_0$.

overlooked in Ref. [7], where the same approximation as ours was implemented for normal leads but also used for asymmetric cases.

B. Keldysh approach

To compute the current-voltage characteristics, we now employ the Keldysh Green function technique. This method has become a standard approach by now; for a review, see, e.g., Ref. [25]. The Keldysh Green function for the d fermion is defined as

$$\mathcal{G}_{\alpha\alpha'}^{ss'}(t, t') = -i \langle \hat{T}_C [d_{\alpha}(t_s) d_{\alpha'}^{\dagger}(t'_{s'})] \rangle, \quad (4)$$

where α, α' ($s, s' = \pm$) are Nambu (Keldysh) indices, and \hat{T}_C is the time-ordering operator along the familiar Keldysh contour C [25]. Accordingly, t_s denotes a time taken on branch s of the Keldysh contour. Similarly, we define a phonon Keldysh Green function $\mathcal{D}^{ss'}(t, t')$ for the quantity $X = b + b^\dagger$ coupling to the fermion d in Eq. (1). In what follows, we use the check notation ($\check{\mathcal{G}}$) in order to schematically indicate the Keldysh structure. In the case of electron Green functions, this also includes the Nambu structure. Denoting the respective functions for $\lambda = 0$ by $\check{\mathcal{G}}_0$ and $\check{\mathcal{D}}_0$, and using the self-energy diagrams in Fig. 1, the dressed Green functions used in our perturbative approximation follow from the Dyson equation. As we consider only the case $\epsilon_0 = 0$, it can be checked that the 'tadpole' diagram does not contribute.

For the superconducting problem of interest here, it is convenient to use the double Fourier representation

$$\check{\mathcal{G}}(t, t') = \sum_{n,m=-\infty}^{+\infty} \int_F \frac{d\omega}{2\pi} e^{-i\omega_n t + i\omega_m t'} \check{\mathcal{G}}_{nm}(\omega), \quad (5)$$

and likewise for all other Green functions and self energies. Here we use

$$\omega_n = \omega + nV \quad (6)$$

for ω within the 'fundamental' domain F defined as

$$F \equiv [-V/2, V/2]. \quad (7)$$

For fixed $\omega \in F$, the Dyson equations then lead to the

matrix equations

$$\check{\mathcal{G}}_{0,nm}^{-1}(\omega) = \delta_{nm}\omega_n\check{\tau}_z - \Gamma \sum_{j=L/R} \check{\gamma}_{j,nm}(\omega) \quad (8)$$

$$\check{\mathcal{G}}^{-1} = \check{\mathcal{G}}_0^{-1} - \check{\Sigma}, \quad \check{\mathcal{D}}^{-1} = \check{\mathcal{D}}_0^{-1} - \check{\Pi}, \quad (9)$$

where the Pauli matrix $\check{\tau}_z$ acts in Keldysh space, and

$$\check{\mathcal{D}}_{0,nm}^{-1}(\omega) = \delta_{nm}\check{\tau}_z \frac{\omega_n^2 - \omega_0^2}{2\omega_0}. \quad (10)$$

The self energy due to tracing out the respective lead is given by the Nambu matrix

$$\check{\gamma}_{j=L/R=\pm,nm}(\omega) = \begin{pmatrix} \delta_{nm} \check{X}(\omega_n \mp V/2) & \delta_{m,n\mp 1} \check{Y}(\omega_n \mp V/2) \\ \delta_{m,n\pm 1} \check{Y}(\omega_n \pm V/2) & \delta_{nm} \check{X}(\omega_n \pm V/2) \end{pmatrix} \quad (11)$$

with Keldysh matrices $\check{Y}(\omega) = -\Delta\check{X}(\omega)/\omega$ and

$$\check{X}(\omega) = \begin{cases} -\frac{\omega}{\sqrt{\Delta^2 - \omega^2}} \check{\tau}_z, & |\omega| < \Delta \\ \frac{i|\omega|}{\sqrt{\omega^2 - \Delta^2}} \begin{pmatrix} 2f_\omega - 1 & -2f_\omega \\ 2f_{-\omega} & 2f_\omega - 1 \end{pmatrix}, & |\omega| > \Delta \end{cases}$$

where $f_\omega = 1/(1 + e^{\omega/k_B T})$ is the Fermi function.

Figure 1 yields for the polarization $\check{\Pi}$ and the self energy $\check{\Sigma}$ the following explicit expressions:

$$\check{\Pi}_{nm}^{ss'}(\omega) = -i\lambda^2 \text{tr} \sum_{n'm'} \int_F \frac{d\omega'}{2\pi} (\check{\tau}_K \check{\mathcal{G}}_{0;n'm'}(\omega') \check{\tau}_K)^{ss'} \times \check{\mathcal{G}}_{0;m'-m,n'-n}^{s's}(\omega' - \omega), \quad (12)$$

$$\check{\Sigma}_{nm}^{ss'}(\omega) = i\lambda^2 \sum_{n'm'} \int_F \frac{d\omega'}{2\pi} \mathcal{D}_{n-n',m-m'}^{ss'}(\omega - \omega') \times (\check{\tau}_K \check{\mathcal{G}}_{0;n'm'}(\omega') \check{\tau}_K)^{ss'}, \quad (13)$$

where 'tr' extends over Nambu space only and $\check{\tau}_K = \check{\tau}_z \sigma_z$. Should the difference $\omega - \omega'$ appearing in Eqs. (12) and (13) fall outside the fundamental domain F , one has to fold it back to F . This is implicitly understood in the above equations.

The steady-state d.c. current through the left/right junction then follows in the form

$$I_{L/R} = \mp 2\Gamma \text{Re} \sum_{nm} \int_F \frac{d\omega}{2\pi} \text{tr} [\sigma_z \check{\gamma}_{L/R,nm}(\omega) \check{\mathcal{G}}_{mn}(\omega)]^{+-}. \quad (14)$$

This relation constitutes a generalization of the Meir-Wingreen formula [26] to the case of superconducting leads. We also define the phonon contribution

$$\delta I_{ph} \equiv I(\lambda) - I(\lambda = 0). \quad (15)$$

Current conservation, $I_L = I_R \equiv I$, can be explicitly verified as follows. In the particle-hole symmetric case, current conservation requires that

$$\check{\mathcal{G}}_{nm}^{ss'}(\omega) = -\sigma_z \check{\mathcal{G}}_{mn}^{s's}(-\omega) \sigma_z. \quad (16)$$

This relation is indeed obeyed since the approximate $\check{\Sigma}$ in Eq. (13) also fulfills Eq. (16).

Using Eq. (14), we evaluate the I - V characteristics for $\lambda = 0.15\Gamma$ (unless noted otherwise) and $k_B T/\Delta = 0.01$. We truncate the summations such that $|\omega_n| < \omega_c = 20\Delta$; further increase of the bandwidth ω_c did not change results. In practice, the domain F in Eq. (7) must be discretized. Typically, we found $\delta\omega = 0.008\Delta$ to be sufficient for convergence. The matrix inversions in Eqs. (8) and (9) are then done for each $\omega \in F$ separately, involving matrix dimensions of the order ω_c/eV . For very small eV/Δ , this becomes quite costly, and we limit ourselves to $eV/\Delta > 0.15$ in the following.

Fortunately, there are several nontrivial tests that we can use to check the scheme. For $\lambda = 0$, our approach quantitatively reproduces the results of Refs. [17, 19, 21]. For $\Delta = 0$, we recover results of Ref. [7] when applicable (i.e., for $\epsilon_0 = 0$). As additional check, Green function sum rules [25] were verified, such as

$$\text{tr} (\tau_K \check{\mathcal{G}}(t, t)) = 0 \quad (17)$$

at coinciding times. While such relations must hold for the exact Green function, it is reassuring to verify that our approximation does not lead to violations of sum rules.

Besides the current, we have also monitored the average phonon number $N_{ph} = \langle b^\dagger b \rangle$ and the frequency-dependent phonon distribution function. We find $N_{ph} \lesssim 1$ for $\lambda/\Gamma = 0.15$, in accordance with our assumption of weak electron-phonon coupling. The phonon distribution function revealed renormalizations of the peak position away from ω_0 by a few percent.

To conclude this section, we note that it is possible to establish a close connection between this Keldysh Green function approach and a Landauer scattering approach incorporating inelastic transitions. Such an 'inelastic MAR' picture will in fact be essential in interpreting our numerical results in Sec. III A. This connection is detailed in the Appendix.

III. RESULTS

A. Subgap regime: Inelastic MAR

Let us then turn to results for the I - V curve. We start with the subgap regime, where MAR provides the dominant transport mechanism. In particular, for $2\Delta/(n+1) < eV < 2\Delta/n$ (n integer), there is a total number n of Andreev reflections for electrons or holes within the superconducting gap. The I - V curve for $\Gamma = 2\Delta$ and $\omega_0 = 0.2\Delta$ is given in Fig. 2, where δI_{ph} is always negative. Note that in this fully transmitting limit, the I - V curve for $\lambda = 0$ is smooth and does not exhibit the MAR 'cusps' encountered at lower transmission [17]. Phonons now restore such features near MAR onsets, with pronounced *even-odd 'parity' effects*: For even

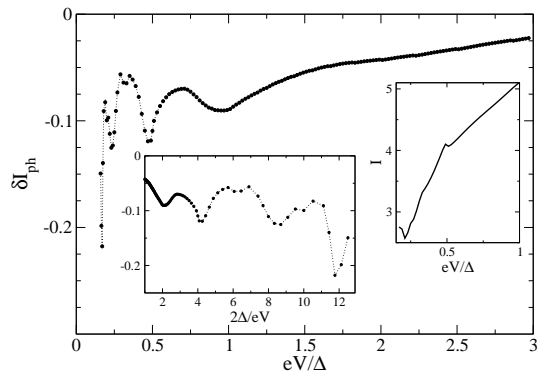


FIG. 2: Phonon difference current (15) for $\hbar\omega_0 = 0.2\Delta$ and $\Gamma = 2\Delta$. In all figures, currents are given in units of $e\Delta/(2\pi\hbar)$, and dotted lines are guides to the eye only. Left inset: Same as function of $2\Delta/eV$. Right inset: Part of the total I - V curve (note the scales).

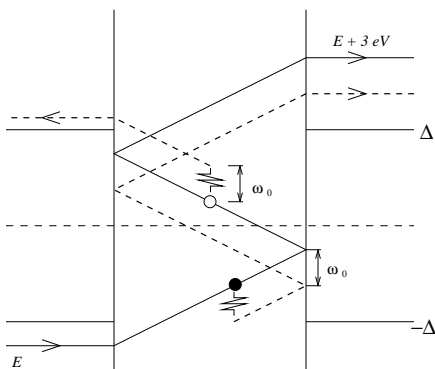


FIG. 3: MAR ladder picture with phonon emission. Here eV is slightly below Δ : for an electron incoming from the left side, we have one hole (open circle) and two electron (filled circle) segments. Dashed lines indicate possible trajectories after single phonon emission involving either hole or electron segments. There is also a MAR path (not shown) for a hole entering from the right side, with one electron and two hole segments.

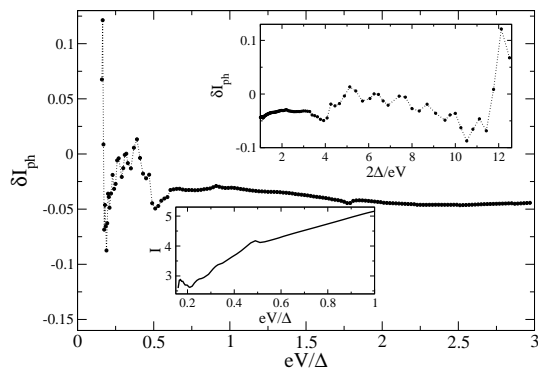


FIG. 4: Same as Fig. 2 but for $\hbar\omega_0 = 1.8\Delta$. The upper inset gives δI_{ph} as a function of $2\Delta/eV$, the lower inset gives the low-voltage part of the total current.

(odd) n , δI_{ph} shows valleys (peaks) around $eV = 2\Delta/n$. This is clearly seen in the left inset of Fig. 2 for n up to 12 [27]. Note that the dip at $n = 8$ is somewhat shifted, presumably due to phonon renormalization effects. However, the appearance of even-odd parity oscillations is quite distinct and surprisingly regular given the complexity of this system.

In order to achieve a physical understanding of this even-odd effect, it is useful to invoke a MAR ladder picture in energy space, including inelastic transitions caused by phonon emission. A schematic description of the MAR ladder picture in this limit is given in Fig. 3. Superconductor spectra are placed next to each other, but because of the presence of the bias, electrons emitted from left to right gain an energy eV in this process. Holes that are reflected, traveling from right to left, also gain this energy.

Usually the scattering approach is used to develop this picture [21], but its straightforward implementation encounters conceptual difficulties in the presence of inelastic phonon transitions. Fortunately, a different route resolving these difficulties can be formulated via the above Keldysh approach, whose formal justification is detailed in the Appendix. Here electron and hole propagators in energy space are coupled to each other through suitable Andreev reflection matching conditions and the phonon self energy $\tilde{\Sigma}$. For a qualitative explanation of the even-odd effect found in the full calculation, cp. Fig. 2, it is sufficient to restrict the full MAR ladder picture to *single* phonon emission processes, where electrons (holes) lose (gain) the energy $\hbar\omega_0$. Since $N_{ph} \lesssim 1$, emission dominates over absorption and multi-phonon processes are rare.

In Fig. 3, the two superconductors are positioned at the same chemical potential, but electrons (from left to right) and holes (from right to left) ‘climb’ the MAR ladder by gaining eV for each Andreev reflection. The higher the total number of Andreev reflections in one cycle, the larger the total charge transmitted. Since we consider the high transmission limit where high-order MAR processes are not penalized, the current is therefore expected to increase (decrease) if phonon emission is able to increase (decrease) the number of Andreev reflections in a MAR cycle. For eV slightly below $2\Delta/n$ with *even* n , we then argue as follows; for $n = 2$, see Fig. 3. For small energy transfer $\hbar\omega_0$, if a phonon is emitted during an electron segment, MAR trajectories in energy space are not drastically modified in the sense that the number of Andreev reflections stays unaffected. However, if a phonon transition occurs during a hole segment, the MAR ladder is shifted upwards by $\hbar\omega_0$ and the last hole on the MAR ladder can be scattered into the continuum (left electrode in Fig. 3) instead of being Andreev reflected. Consequently, one Andreev reflection is lost and hence the current is expected to decrease. This argument applies both to incoming electrons and holes, and explains why current valleys are observed for $eV \approx 2\Delta/n$ with even n in Fig. 2. On the other hand, consider eV slightly

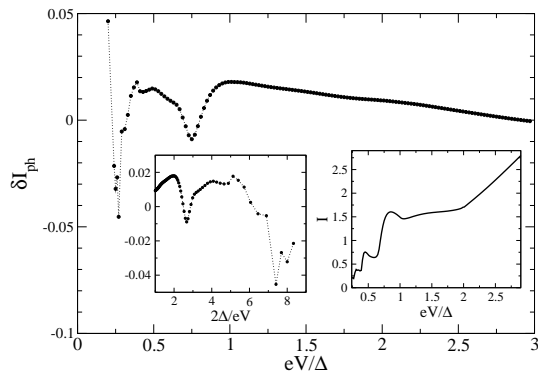


FIG. 5: Same as Fig. 2 but for $\Gamma = 0.5\Delta$. The left inset gives δI_{ph} versus $2\Delta/eV$, the right inset the total current.

above $2\Delta/n$ with *odd* n . Reiterating the above analysis, now phonon emission during a hole segment tends not to affect the number of Andreev reflections. If the phonon is emitted during an electron segment, however, an additional Andreev reflection has to take place to complete the MAR cycle, leading to a current peak for $eV \approx 2\Delta/n$ with odd n .

Next consider $\hbar\omega_0 = 1.8\Delta$ but otherwise identical parameters, see Fig. 4, where δI_{ph} can be positive and again shows oscillations near the MAR onsets, which are less pronounced for small $n = 2\Delta/eV$. Remarkably, even for small voltages, $eV \ll \hbar\omega_0$, a rather complicated subgap structure is caused by the phonon. At such low voltages, this is only possible via MAR, for otherwise electrons or holes do not have enough energy to emit a phonon. The broad minimum corresponding to $n = 2$ observed in Fig. 2 has now vanished. Let us invoke the MAR ladder picture to rationalize this effect. For $eV \lesssim \Delta$, by emitting a *high-energy* phonon ($\hbar\omega_0 > \Delta$), the last electron on the MAR ladder can now be scattered back inside the gap instead of heading to the continuum. This increases the number of reflections and thus the current. As a phonon emitted during the hole segment has the opposite effect (see above), the net outcome of the higher phonon frequency is to suppress the valley at $eV \approx \Delta$ expected for small ω_0 . Figure 4 also shows a dip in the current at $eV \approx 1.8\Delta$, representing a phonon backscattering feature at $eV = \hbar\omega_0$. The scaling of this dip with ω_0 was confirmed by additional calculations. One can also see a two-phonon feature at $eV = \hbar\omega_0/2$ in Fig. 4.

Let us then briefly go back to $\hbar\omega_0 = 0.2\Delta$ (cp. Fig. 2), but now for $\Gamma = 0.5\Delta$, see Fig. 5. For small Γ , quasi-resonances appear [21] and cause additional features, e.g. negative differential conductance portions in the I - V curve. The MAR ladder picture then has to include both quasi-resonances (cp. Ref. [21]) and phonon transitions, which is possible but beyond the scope of this paper. Fig. 5 shows that the even-odd parity effect requires large Γ to be observable.

B. Excess and Josephson current

Finally, we briefly discuss the limits of very large and/or zero voltage. Starting with the first case (excess current), we have computed the difference $\delta I_{exc,ph}$ between the excess currents I_{exc} with and without the phonon. This calculation has been done at $eV = 10\Delta$, which according to the discussion in Ref. [21] is certainly large enough for our parameters. For the case of high transmission encountered here, we find that phonons generally *enhance* the excess current. To give a concrete example, for $\hbar\omega_0 = 0.8\Delta$, $\Gamma = 2\Delta$ and $\lambda = 0.5\Delta$, we find $\delta I_{exc,ph}/I_{exc} \approx 0.07$. A similar current enhancement at high transmission was also found for environmental Coulomb blockade in superconducting junctions, and has been explained as 'antiblockade' effect [28]. As such, this effect of the phonon may not be too surprising.

Second, the equilibrium Josephson current has been calculated by adopting our approach to the Matsubara representation. For arbitrary parameters, it is straightforward to numerically compute the full current-phase relation. However, the current-phase relation in the adiabatic phonon regime defined by

$$\hbar\omega_0 \ll \Delta \ll \Gamma \quad (18)$$

can even be calculated analytically, with the result

$$I(\phi) = (e\Delta^2/2\hbar) T_0 \sin(\phi)/E_0(\phi), \quad (19)$$

where

$$E_0(\phi) = \Delta[1 - T_0 \sin^2(\phi/2)]^{1/2} \quad (20)$$

is an Andreev bound state energy [17] in the junction with an effective transparency

$$T_0 = \frac{1}{1 + \lambda^2/4\Gamma^2}. \quad (21)$$

The ϕ -dependent shift without any broadening of the Andreev level caused by the coupling to a phonon mode is characteristic for the coherent limit and decreases the critical current. Very similar results were reported in Ref. [22] in the opposite limit $\Gamma \ll \Delta$.

IV. CONCLUSIONS

In this work, we have for the first time theoretically explored nonequilibrium molecular transport with superconducting leads in the coherent phonon regime. Phonons reveal a rich subgap structure even for voltages well below the phonon frequency, including a surprising even-odd parity effect near the MAR onsets. This effect can be largely understood within a physically appealing inelastic MAR ladder picture, based on the assumption that single phonon emission processes dominate. For stronger electron-phonon couplings, also multiple phonon

processes and/or absorption becomes important, and the practical usefulness of such a scattering approach is less clear, although it can be formally derived as outlined in the Appendix.

Let us also offer a brief outlook. Besides the obvious interest to experimentally probe the effects predicted here, the problems raised above deserve further theoretical work. In the case of strong electron-phonon coupling, different approximations will be necessary. Moreover, other quantities such as shot noise or frequency-dependent noise [29] deserve attention. Noise can yield information about the effective charge involved in the transfer process, and how this charge is affected by phonon transitions remains to be explored. It would also be interesting to formalize the notion of inelastic MAR spectroscopy, potentially allowing to infer the electronic structure of molecules from the superconducting current-voltage characteristics. Such approaches have already been very useful in nanoscale break junctions, and are of obvious interest in the molecular electronics context as well. It is safe to conclude that superconducting molecular transport definitely warrants further surprises in the future.

Acknowledgments

We thank K. Flensberg, A. Levy-Yeyati, and V. Shumeiko for useful discussions. R.E. and C.M. are grateful to the CPT for hospitality. R.E. was supported by the CNRS, the ESF network INSTANS, and by the EU networks HYSWITCH and DIENOW. T.M. acknowledges support from an A.C. Nanoscience from CNRS.

INELASTIC MAR: SCATTERING APPROACH

In this appendix, we outline the derivation of the Landauer scattering approach to inelastic MAR incorporating phonon transitions. Such an approach is formulated here using the equation-of-motion method, where transfer matrices are expressed in terms of Keldysh Green functions. This provides a formal justification for the intuitive MAR ladder picture used in Sec. III A.

Using the Hamiltonian (1), we can write down the equations of motion for the quasiclassical envelope function $\Psi_{j,k}^{(r)}$ describing right/left-moving quasiparticles ($r = \pm$) in the left or right lead ($j = L/R = \pm$) with momentum $r k_F + k$. Here $|k| \ll k_F$ is assumed, and with the Fermi velocity v_F , we obtain

$$(i\partial_t - r k v_F \sigma_z - \Delta \sigma_x) \Psi_{j=\pm,k}^{(r)}(t) = t_0 \sigma_z e^{\pm i \sigma_z V t / 2} d(t). \quad (22)$$

Similarly, the equation of motion for the molecular fermion (Nambu spinor d) is

$$(i\partial_t - \lambda X(t) \sigma_z) d(t) = t_0 \sigma_z \sum_{j=\pm,r} e^{\mp i \sigma_z V t / 2} \Psi_j^{(r)}(t), \quad (23)$$

where $\Psi_j^{(r)} \equiv \sum_k \Psi_{jk}^{(r)}$. Here we consider the simplest possible situation, where phonon renormalization effects like the polarization bubble in Fig. 1 are completely disregarded. In that case it is sufficient to simply take an equilibrium average over the phonon subsystem, while otherwise one should also take into account the equation of motion for $X(t)$.

The solution of Eq. (22), adapted to $\Psi_j^{(r)}(t)$, can be written as the sum of a free (homogeneous) solution $\Psi_{j0}^{(r)}(t)$, describing an incoming quasiparticle in lead $j = L/R$, plus a scattered part due to the interaction with the molecular level,

$$\Psi_j^{(r)}(t) = \Psi_{j0}^{(r)}(t) + t_0 \int dt' g_j^{(r)}(t-t') \times \sigma_z e^{\pm i \sigma_z V t' / 2} d(t'), \quad (24)$$

which is expressed in terms of the retarded Green function $g_j^{(r)}$ for uncoupled electrodes whose Fourier transform is given by

$$g_L^{(\pm)}(\omega) = g_R^{(\mp)}(\omega) = \frac{\pi \nu_0}{2i} \left(\frac{\omega + \Delta \sigma_x}{\sqrt{(\omega + i0)^2 - \Delta^2}} \mp \sigma_z \right).$$

When summed over r , this essentially yields the retarded components of $\tilde{\gamma}_j$ in Sec. II.

In what follows, we use $s = \{1, 2, 3, 4\}$ in order to label scattering processes corresponding to electron- or hole-like quasiparticles incoming from the left ($s = 1, 2$) or right ($s = 3, 4$) electrode. In Fourier representation, where E is the energy of the incoming quasiparticle ($|E| > \Delta$) and $E_n = E + nV$, we write

$$\Psi_j^{(r)}(t) = \sum_n e^{-i E_n t} \begin{pmatrix} u_{jn}^{(r)} \\ v_{jn}^{(r)} \end{pmatrix} \quad (25)$$

and introduce electron- and hole-type spinors,

$$\Phi_{jn}^e \equiv \begin{pmatrix} u_{jn}^{(+)} \\ u_{jn}^{(-)} \end{pmatrix}, \quad \Phi_{jn}^h \equiv \begin{pmatrix} v_{jn}^{(+)} \\ v_{jn}^{(-)} \end{pmatrix}.$$

These spinors are defined on a chiral space, with the two entries corresponding to the right- and left-moving parts. From Eq. (24), we proceed to derive a first set of Andreev reflection matching equations for $\Phi_{jn}^{e,h}$,

$$\begin{aligned} \Phi_{Ln}^e &= \begin{pmatrix} a_n & 0 \\ 0 & a_n^{-1} \end{pmatrix} \Phi_{Ln}^h + \delta_{n0} (u_E^2 - v_E^2) \begin{pmatrix} \delta_{s1}/u_E \\ -\delta_{s2}/v_E \end{pmatrix} \\ \Phi_{Rn}^e &= \begin{pmatrix} a_n^{-1} & 0 \\ 0 & a_n \end{pmatrix} \Phi_{Rn}^h + \delta_{n0} (u_E^2 - v_E^2) \begin{pmatrix} -\delta_{s4}/v_E \\ \delta_{s3}/u_E \end{pmatrix}, \end{aligned}$$

where $a_n = (E_n - \sqrt{(E_n + i0)^2 - \Delta^2})/\Delta$. Furthermore, the u_E, v_E denote the $n = 0$ entries in Eq. (25). Note that these matching equations are not modified by the presence of phonons, see Ref. [30].

Iterating Eq. (23) and averaging over the phonons, we find

$$(i\partial_t - \Sigma) \circ d = t_0 \sigma_z \sum_{j=\pm, r} e^{\mp i\sigma_z V t/2} \Psi_j^{(r)}(t), \quad (26)$$

where \circ is a shorthand for convolution. The phonon self energy entering Eq. (26) is given by

$$\Sigma(t, t') = i\lambda^2 \mathcal{D}_0^>(t, t') \sigma_z \mathcal{G}_0^R(t, t') \sigma_z. \quad (27)$$

Note that this ignores the polarization-bubble renormalization, see above. For the four different scattering processes indexed by s , it is convenient to introduce matrices $\tilde{\Sigma}_{nm}$ according to

$$\begin{aligned} \tilde{\Sigma}(t, t') &= e^{i\sigma_z \sigma_s t V/2} \sigma_z \Sigma(t, t') \sigma_z e^{-i\sigma_z \sigma_s t' V/2} \\ &\equiv \sum_{nm} \int_F \frac{d\omega}{2\pi} e^{-i\omega_n t + i\omega_m t'} \tilde{\Sigma}_{nm}(\omega) \end{aligned} \quad (28)$$

with $\sigma_s = 1$ ($\sigma_s = -1$) for $s \in \{1, 2\}$ ($s \in \{3, 4\}$). To keep the notation simple, the s -dependence of $\tilde{\Sigma}_{nm}$ is not exhibited explicitly.

Using Eq. (26), we then obtain a second set of matching equations. For $s = \{1, 2\}$,

$$\begin{aligned} \Phi_{R, n+1}^e &= (T_n^e)^{-1} \Phi_{L_n}^e + \sum_m (S_{nm}^{ee} \Phi_{L_m}^e + S_{nm}^{eh} \Phi_{L_m}^h) \\ \Phi_{R, n-1}^h &= (T_n^h)^{-1} \Phi_{L_n}^h + \sum_m (S_{nm}^{hh} \Phi_{L_m}^h + S_{nm}^{he} \Phi_{L_m}^e), \end{aligned}$$

while for $s = \{3, 4\}$,

$$\begin{aligned} \Phi_{L, n-1}^e &= T_{n-1}^e \Phi_{R_n}^e + \sum_m (S_{nm}^{ee} \Phi_{R_m}^e + S_{nm}^{eh} \Phi_{R_m}^h) \\ \Phi_{L, n+1}^h &= T_{n+1}^h \Phi_{R_n}^h + \sum_m (S_{nm}^{hh} \Phi_{R_m}^h + S_{nm}^{he} \Phi_{R_m}^e). \end{aligned}$$

Here, electron/hole transfer matrices are given by

$$T_n^{e/h} = \begin{pmatrix} 1/t_n^{e/h} & (r_n^{e/h}/t_n^{e/h})^* \\ r_n^{e/h}/t_n^{e/h} & 1/t_n^{e/h*} \end{pmatrix} \quad (29)$$

with

$$t_n^{e/h} = -1/(1 \mp iE_n^{e/h}/2\Gamma), \quad r_n^{e/h}/t_n^{e/h} = \pm iE_n^{e/h}/2\Gamma,$$

where $E_n^{e/h} = E + (n \pm 1/2)V$. Furthermore, transfer matrices linked to phonon-induced transitions are given in terms of the phonon self-energy matrix elements introduced in Eq. (28)

$$\begin{aligned} \begin{pmatrix} S_{nm}^{ee} & S_{nm}^{eh} \\ S_{nm}^{he} & S_{nm}^{hh} \end{pmatrix} &= \frac{i\sigma_s}{2\Gamma} (\tau_z - i\tau_y) \\ &\times \begin{pmatrix} -\tilde{\Sigma}^{11}(E) & \tilde{\Sigma}^{12}(E) \\ -\tilde{\Sigma}^{21}(E) & \tilde{\Sigma}^{22}(E) \end{pmatrix}_{nm}, \end{aligned} \quad (30)$$

where the Pauli matrices $\tau_{y,z}$ operate in the space of the $\Phi^{e,h}$ spinors and the α indices in $\tilde{\Sigma}^{\alpha\alpha'}$ refer to Nambu space. Note again that these quantities all carry an implicit s -dependence.

Finally, after straightforward but somewhat tedious algebra, the d.c. current is expressed in terms of the above scattering states,

$$\begin{aligned} I &= ev_F \int_{|E|>\Delta} dE \frac{|E|}{\sqrt{E^2 - \Delta^2}} f_E \sum_{s=1}^4 \sum_n \\ &\times \sum_{a=e/h} \left[(\delta_{s1} + \delta_{s2}) \Phi_{Rn}^{a\dagger}(E) \tau_z \Phi_{Rn}^a(E) \right. \\ &\left. + (\delta_{s3} + \delta_{s4}) \Phi_{Ln}^{a\dagger}(E) \tau_z \Phi_{Ln}^a(E) \right]. \end{aligned} \quad (31)$$

Similarly, the full Keldysh Green function $\tilde{\mathcal{G}}$ can also be constructed from the complete set of scattering states $\Phi_{jn}^{e,h}(E)$.

-
- [1] A. Nitzan and M.A. Ratner, *Science* **300**, 1384 (2003).
[2] G. Cuniberti, G. Fagas, and K. Richter (eds.), *Introducing Molecular Electronics*, Lect. Notes Phys. 680 (Springer 2005).
[3] M. Tsukada, K. Tagami, K. Hirose, and N. Kobayashi, *J. Phys. Soc. Jpn.* **74**, 1079 (2005).
[4] D. Boese and H. Schoeller, *Europhys. Lett.* **54**, 668 (2001).
[5] K. Flensberg, *Phys. Rev. B* **68**, 205323 (2003); S. Braig and K. Flensberg, *Phys. Rev. B* **68**, 205324 (2003)
[6] J. Koch and F. von Oppen, *Phys. Rev. Lett.* **94**, 206804 (2005).
[7] A. Mitra, I. Aleiner, and A.J. Millis, *Phys. Rev. B* **69**, 245302 (2004).
[8] P.S. Cornaglia, H. Ness, and D.R. Grempel, *Phys. Rev. Lett.* **93**, 147201 (2004); P.S. Cornaglia, D.R. Grempel, and H. Ness, *Phys. Rev. B* **71**, 075320 (2005).
[9] M.R. Buitelaar, W. Belzig, T. Nussbaumer, B. Babic, C. Bruder, and C. Schönberger, *Phys. Rev. Lett.* **91**, 057005 (2003).
[10] A.Yu. Kasumov, R. Deblock, M. Kociak, B. Reulet, H. Bouchiat, I.I. Khodos, Yu.B. Gorbatov, V.T. Volkov, C. Journet, and M. Burghard, *Science* **284**, 1508 (1999).
[11] B. Reulet, A.Yu. Kasumov, M. Kociak, R. Deblock, I.I. Khodos, Yu.B. Gorbatov, V.T. Volkov, C. Journet, and H. Bouchiat, *Phys. Rev. Lett.* **85**, 2829 (2000).
[12] P. Jarillo-Herrero, J.A. van Dam, and L.P. Kouwenhoven, *Nature* **439**, 953 (2006).

- [13] K. Grove-Rasmussen, H.I. Jorgensen, and P.E. Lindelof, cond-mat/0601371.
- [14] A.Yu. Kasumov *et al.*, Phys. Rev. B **72**, 033414 (2005).
- [15] T.M. Klapwijk, G.E. Blonder, and M. Tinkham, Physica (Amsterdam) 109B-110B, 1657 (1982).
- [16] G.B. Arnold, J. Low Temp. Phys. **68**, 1 (1987).
- [17] E.N. Bratus, V.S. Shumeiko, and G. Wendin, Phys. Rev. Lett. **74**, 2110 (1995)
- [18] D. Averin and A. Bardas, Phys. Rev. Lett. **75**, 1831 (1995).
- [19] J.C. Cuevas, A. Martin-Rodero, and A.L. Yeyati, Phys. Rev. B **54**, 7366 (1996).
- [20] A.L. Yeyati, J.C. Cuevas, A. López-Dávalos, and A. Martin-Rodero, Phys. Rev. B **55**, R6137 (1997).
- [21] G. Johansson, E.N. Bratus, V.S. Shumeiko, and G. Wendin, Phys. Rev. B **60**, 1382 (1999).
- [22] T. Novotny, A. Rossini, and K. Flensberg, Phys. Rev. B **72**, 224502 (2005).
- [23] G. Baym and L.P. Kadanoff, Phys. Rev. **124**, 287 (1961); G. Baym, Phys. Rev. **127**, 1391 (1962).
- [24] S. Hershfield, J.H. Davies, and J.W. Wilkins, Phys. Rev. B **46**, 7046 (1992); T. Frederiksen, M. Brandbyge, N. Lorente, and A.P. Jauho, Phys. Rev. Lett. **93**, 256601 (2004).
- [25] A. Kamenev, in *Nanophysics: Coherence and Transport* Les Houches session LXXXI, ed. by H. Bouchiat *et al.* (Elsevier, 2005).
- [26] Y. Meir and N.S. Wingreen, Phys. Rev. Lett. **68**, 2512 (1992).
- [27] The accuracy of the curve (see especially the left inset) is somewhat compromised for large n because a voltage grid of constant stepsize has been used.
- [28] A. Levy Yeyati, J.C. Cuevas, and A. Martin-Rodero, Phys. Rev. Lett. **95**, 056804 (2005).
- [29] P.-M. Billangeon, F. Pierre, H. Bouchiat, and R. Deblock, Phys. Rev. Lett. **96**, 136804 (2006).
- [30] G. Johansson, G. Wendin, K.N. Bratus, and V.S. Shumeiko, Superlatt. Microstructures **25**, 905 (1999).